

THE GALAXY DISTRIBUTION FUNCTION FROM THE 2MASS SURVEY

GREGORY R. SIVAKOFF

Department of Astronomy, University of Virginia, P. O. Box 3818, Charlottesville, VA 22903-0818; grs8g@virginia.edu

AND

WILLIAM C. SASLAW

Department of Astronomy, University of Virginia, P. O. Box 3818, Charlottesville, VA 22903-0818; Institute of Astronomy, Cambridge, England; and National Radio Astronomy Observatory¹, Charlottesville, VA; wcs@virginia.edu

ABSTRACT

We determine the spatial distribution function of galaxies from a wide range of samples in the 2MASS survey. The results agree very well with the form of the distribution predicted by the theory of cosmological gravitational many-body galaxy clustering. On large scales we find a value of the clustering parameter $b = 0.867 \pm 0.026$, in agreement with $b = 0.83 \pm 0.05$ found previously for the Pisces-Perseus supercluster. We measure $b(\theta)$ as a function of scale, since this is a powerful test of the applicability of computer simulations. The results suggest that when galaxies clustered they were usually surrounded by individual, rather than by communal haloes.

Subject headings: large-scale structure of universe — dark matter — gravitation — infrared: galaxies — galaxies: clusters: general — galaxies: statistics

1. INTRODUCTION

The spatial locations of galaxies may be described by many different statistics. These include distribution functions, low order correlation functions, multi-fractal dimensions, topological genus, power spectra, spherical harmonics, multipoles, minimal spanning trees, percolation and moments. All these statistics are related and each emphasizes different aspects of the distribution (e.g., Saslaw 2000). Here we determine the observed galaxy distribution function from the 2MASS Catalogs with considerably greater precision than has previously been possible from smaller catalogs, and compare it with theoretical expectations.

The galaxy distribution function contains information about correlations to all orders, about voids and underdense regions, and about clustering over a very wide range of intensities, sizes and shapes. Moreover it can be calculated analytically for cosmological gravitational many-body clustering in both linear and non-linear regimes (Saslaw 2000).

These theoretical calculations assume, consistent with direct N-body simulations, that galaxy clustering evolves through a sequence of quasi-equilibrium states. This occurs because in any overdense region the local dynamical timescale is shorter than the global timescale for evolution of average quantities, such as the overall density, velocity dispersion, and the ratio of gravitational potential correlation energy to the kinetic energy of peculiar velocities. The global timescale for these average ensemble properties to change, becomes even greater than the Hubble time, $R(t)/\dot{R}$, as local partially virialized structures form. The Hubble expansion exactly cancels the long-range gravitational many-body mean field, not only in the usual Einstein-Friedmann models, but also in those models with a cosmological constant and quintessence. For the cosmological constant and quintessence models, one can straightforwardly extend the earlier derivations

(Saslaw 2000; Saslaw & Fang 1996) that applied to the Einstein-Friedmann case.

Under these conditions, the clustering of galaxies, each of which may be surrounded by its own dark matter halo, occurs mainly through their mutual gravitational interactions. This differs from those cold dark matter models that are dominated by very large haloes containing galaxies moving mainly as test particles within the gravitational field of these haloes (e.g. the massive haloes in Fukushige & Makino 2003). When the mutual gravitational interactions of individual galaxies dominate, clustering can be described by quasi-equilibrium thermodynamics (Saslaw 2000; Saslaw & Fang 1996; Saslaw & Hamilton 1984) and statistical mechanics (Ahmad et al. 2002; Leong & Saslaw 2004). This theory applies for a wide range of initial conditions, including initial power law perturbation spectra with $-1 \lesssim n \lesssim 1$ (Itoh 1990). Characterising the complete range of initial conditions that form a basin of attraction for this theory remains an important unsolved problem.

Analysis of the cosmological many-body problem predicted (Saslaw & Hamilton 1984) that its distribution function $f_V(N)$, i.e. the probability that a randomly placed volume V in space contains N galaxies, has the form

$$f_V(N) = \frac{\bar{N}(1-b)}{N!} [\bar{N}(1-b) + Nb]^{N-1} e^{-[\bar{N}(1-b) + Nb]}, \quad (1)$$

where

$$\bar{N} = \bar{n} V \quad (2)$$

is the expected number for an average number density \bar{n} . The strength of clustering is measured by

$$b = -\frac{W}{2K} = \frac{2\pi Gm^2\bar{n}}{3T} \int_V \xi(\bar{n}, T, r) \frac{1}{r} r^2 dr \quad (3)$$

for a spherical volume where W is the gravitational correlation energy, K is the kinetic energy of galaxy peculiar velocities indicating an ensemble average temperature T ,

arXiv:astro-ph/0503509v1 24 Mar 2005

¹ Operated by Associated Universities, Inc., under cooperative agreement with the National Science Foundation.

the average galaxy mass is m , and ξ is the two-galaxy correlation function. Since the volume V may be a cone with apex at the observer which projects the galaxies in its volume into a cell of area A on the sky, the same form of the distribution function in equation (1) applies to counts of galaxies in two-dimensional cells on the sky. This form of equation (3) assumes that evolution is negligible within the volume, which is reasonable for a narrow redshift band as in the 2MASS catalog ($0 \leq z \lesssim 0.1$). For volumes covering wide redshift bands, evolution may be included as described in Fang & Saslaw (1997) and Saslaw & Edgar (2000).

Although the form of equation (1) is independent of the shape and size of randomly located volumes which are not pathological (e.g., not fractal or chosen to avoid galaxies), the value of b will depend on volume and shape. This was found in early N-body simulations (Itoh et al. 1988) and explicitly calculated for square projected cones using equation (3) (Lahav & Saslaw 1992). Comparisons of different values of \bar{N} and b for cells of the same shape and size, but for different subsamples of galaxies, can be used to explore possible biases in these subsamples. If the bias is known *a priori*, it can be incorporated into equations (1) and (3) as described in detail previously (Lahav & Saslaw 1992; Saslaw 2000). In principle, an unknown bias contained in subsamples can also be recovered from the results, but its uniqueness is more difficult to establish.

The value of \bar{N} can be determined directly from the catalog and the value of b follows for equation (1) from the observed variance of counts in cells of any particular volume and shape:

$$\langle (\Delta N)_V^2 \rangle = \frac{\bar{N}}{(1 - b(V))^2}. \quad (4)$$

Therefore in principle the theory contains no free parameters for comparing equation (1) with the observations. We can also fit \bar{N} and b in equation (1) directly to the observed distribution function, and see if the slight difference between these two methods of determining \bar{N} and b provides useful information.

After deriving equation (1), its predicted form was found to agree well with counts in cells and void probabilities in several galaxy surveys including the Zwicky Catalog (Saslaw & Crane 1991), the UGC and ESO Catalogs (Lahav & Saslaw 1992) and the IRAS Catalog (Sheth et al. 1994), all projected onto the sky, as well as for the SSRS Catalog (Fang & Zou 1994), and the Pisces-Perseus Supercluster (Saslaw & Haque-Copilah 1998) in three dimensions. All previous comparisons have involved catalogs containing at most several tens of thousands of galaxies. The new catalogs becoming available have about 10–100 times as many galaxies, with different levels of sky coverage, homogeneity, and information about galaxy properties.

These new larger catalogs are important because their improved statistics may reveal departures from equation (1) resulting from different distributions of galaxies and dark matter, merging, mass segregation, or other environmental effects. Section 2 describes the 2MASS Catalog and our method of analysis, Section 3 gives our results, and Section 4 describes some of their implications.

2. THE 2MASS CATALOG AND ITS ANALYSIS

The Two Micron All Sky Survey employed telescopes in the Northern and Southern hemispheres to observe in the three infrared bands J ($1.11 - 1.36\mu m$), H ($1.50 - 1.80\mu m$) and K_s ($2.00 - 2.32\mu m$). Most of the sources are points, but 1,647,599 are resolved with respect to the observed 2MASS point spread function and they constitute the Extended Source Catalog (XSC). About 97% of these extended sources are galaxies². Examination of the Abell 262 cluster suggests that most of the 2MASS galaxies are local with $z \lesssim 0.1$ (Skrutskie, private communication). In addition to the local population, the Catalog contains more distant very luminous galaxies and about 0.4% of the catalog may be quasars with redshifts ≤ 5 (Barkhouse & Hall 2001). The low redshifts for nearly all the sources indicate that evolutionary corrections will not be significant for our statistics using this sample.

To select our samples, we adopted Kron magnitudes following Maller et al. (2005) and dereddened them using the reddening maps of Schlegel et al. (1998) assuming $A(J) = 0.82E(B - V)$, $A(H) = 0.48E(B - V)$, and $A(K_s) = 0.28E(B - V)$ (Majewski et al. 2003)³. We required all galaxies brighter than $K_{s,0} = 12$ to have $J_0 - K_{s,0}$ between 0.7 and 1.4 (Maller et al. 2005) and all candidate galaxies to have star-galaxy separation indices typical of galaxies ($e_{score} < 1.4$ and $g_{score} < 1.4$) to avoid confusion with nearby galactic sources. We also require that a candidate is not listed² as a possible anomaly (e.g. artifact, cluster/galaxy piece, Galactic object or star) and that if a candidate is among the $\sim 25\%$ visually verified sources, it is not indicated as non-extended ($vc \neq 2$). To minimize the relative contribution of stars in the samples, we usually remove cells at low Galactic latitude, $|\delta_{gal}| < 20^\circ$. In some cases we choose higher Galactic latitude cutoffs for comparison, as shown in Table 1 and Figure 3. We also remove cells with high stellar density, or in very dusty regions, as described below. Although this does not explicitly avoid the Magellanic clouds, the high stellar density cutoffs remove their central regions.

To examine the completeness of the galaxy sample, we have measured (V/V_{max}) as a function of $K_{s,0}$ magnitude. The results are essentially constant between about 0.52 and 0.51 for $10.0 < K_{s,0} < 13.7$ and we employ a conservative truncation of the galaxy sample at $K_{s,0} = 13.5$.

To obtain the distribution function from counts-in-cells, we map the sources onto a Hammer-Aitoff equal area projection (e.g., Calabretta & Greisen 2002):

$$\begin{aligned} \gamma &= \frac{180^\circ}{\pi} \sqrt{\frac{2}{1 + \cos \delta \cos(\alpha/2)}}, \\ x &= 2\gamma \cos \delta \sin(\alpha/2), \\ y &= \gamma \sin \delta. \end{aligned} \quad (5)$$

Here (α, δ) is the Galactic coordinate in radians and (x, y) is the projected coordinate. Figure 1 shows the sample of galaxy candidates with $K_{s,0} < 13.5$ on a square-root

² The Explanatory Supplement to the 2MASS All Sky Data Release is available at <http://www.ipac.caltech.edu/2mass/releases/allsky/doc> for this and related information.

³ The corrected magnitudes are denoted by a subscripted 0.

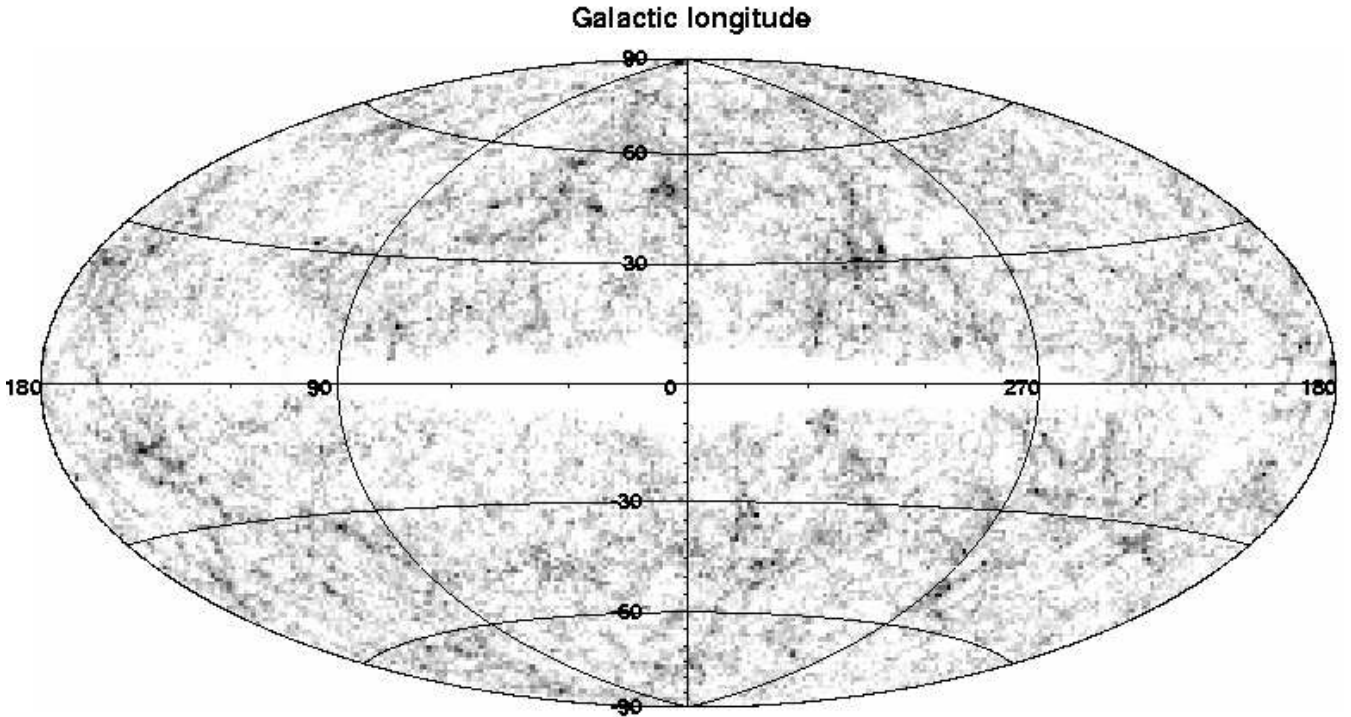


FIG. 1.— Grey-scale image of the density of 663,166 galaxy candidates with $K_{s,0} < 13.5$ in cells of $1^\circ \times 1^\circ$. A square-root stretch having a contrast of 2 was applied with the darkest cells indicating the highest density.

stretched grey scale with the darkest cells indicating the highest density. The extended dense region in the upper right hand (northwest) quadrant is the Shapley Supercluster. This map contains 663,166 galaxy candidates in cells of $1^\circ \times 1^\circ$ on the sky. We then apply two filters. The first is a spatial filter that removes cells below a specified Galactic latitude or on the boundary of the projection. The second filter reduces the probability of confusion with stars by removing cells whose stellar density, n_{st} , is greater than $10^{3.3}$ ($\approx 2000 \text{ deg}^{-2}$) and cells with objects that have $A(K_s) > 0.05$ (Maller et al. 2005). We experimented with a range of stellar density cutoffs and found $n_{st} < 10^{3.3}$ to be the optimum between leaving too few galaxies or including so many stars that a small percentage of them were close enough to each other that they could masquerade as galaxies.

Having determined all the relevant cells, we simply count the number of galaxies in each to construct histograms of the distribution functions for various samples. These filtered samples include essentially the whole sky, four hemispherical sections, and four quadrant sections, along with a range of cell sizes, Galactic latitude cutoffs and magnitude limits. Values of \bar{N} from the average projected density and b_v from the variance of counts in cells in equation (4) are used as a first approximation to determine $f_V(N)$ in equation (1) from the observations. Then we go a step further and find values of \bar{N} and b that minimize a χ^2 fit to the observations. The differences in these values for a single histogram, and among similar histograms in different areas of the sky, give a measure of their global uncertainty. However values of χ^2 cannot be used here for the usual probability estimates that a sample represents a particular distribution function because

the populations of nearby cells are often strongly correlated. Since these cells are not independent, the values of χ^2 are used just to optimize the fitting. To facilitate this, we have combined bins with very small $f_V(N)$ in the tails of the distribution (cf. Kendall & Stuart 1979).

3. RESULTS

To illustrate the relation between the predicted form of $f_V(N)$ in equation (1) and the observed 2MASS galaxy distribution function, Figures 2a- 2f plot least-squares fits of $f_V(N)$ to the observed histograms for square cells of five different size cells on the sky. The areas under these histograms in the bottom panel of each figure illustrate values of $\chi = (f_{obs} - f_{theory})N_{cell}^{1/2}/f_{obs}^{1/2}$, where N_{cell} is the total number of cells evaluated. The $1^\circ \times 1^\circ$ cells in Figures 2c and 2d are representative; in Figure 2d, we have shifted the grid of cells by 0.5° on the sky. This shift slightly alters the detailed shape of the histogram for the probability that a cell has N galaxies, but leaves the best fit values of \bar{N} and b almost unchanged. Thus the exact positioning of the grid is unimportant, which indicates that the galaxy distribution is statistically homogeneous.

In the overall fits there are small differences between the observations and the theoretical distribution of equation (1). The largest differences, as measured by χ , occur in the large N tails where there are relatively few cells. The peaks of the observed distribution function are usually higher than those of equation (1). Since the areas of the distributions have the same normalization, a slight excess for some values of N must be offset by a deficit for other values. This slight deficiency generally occurs between the peak and high N tail of the distribution. There may be several contributions to these differences: the pe-

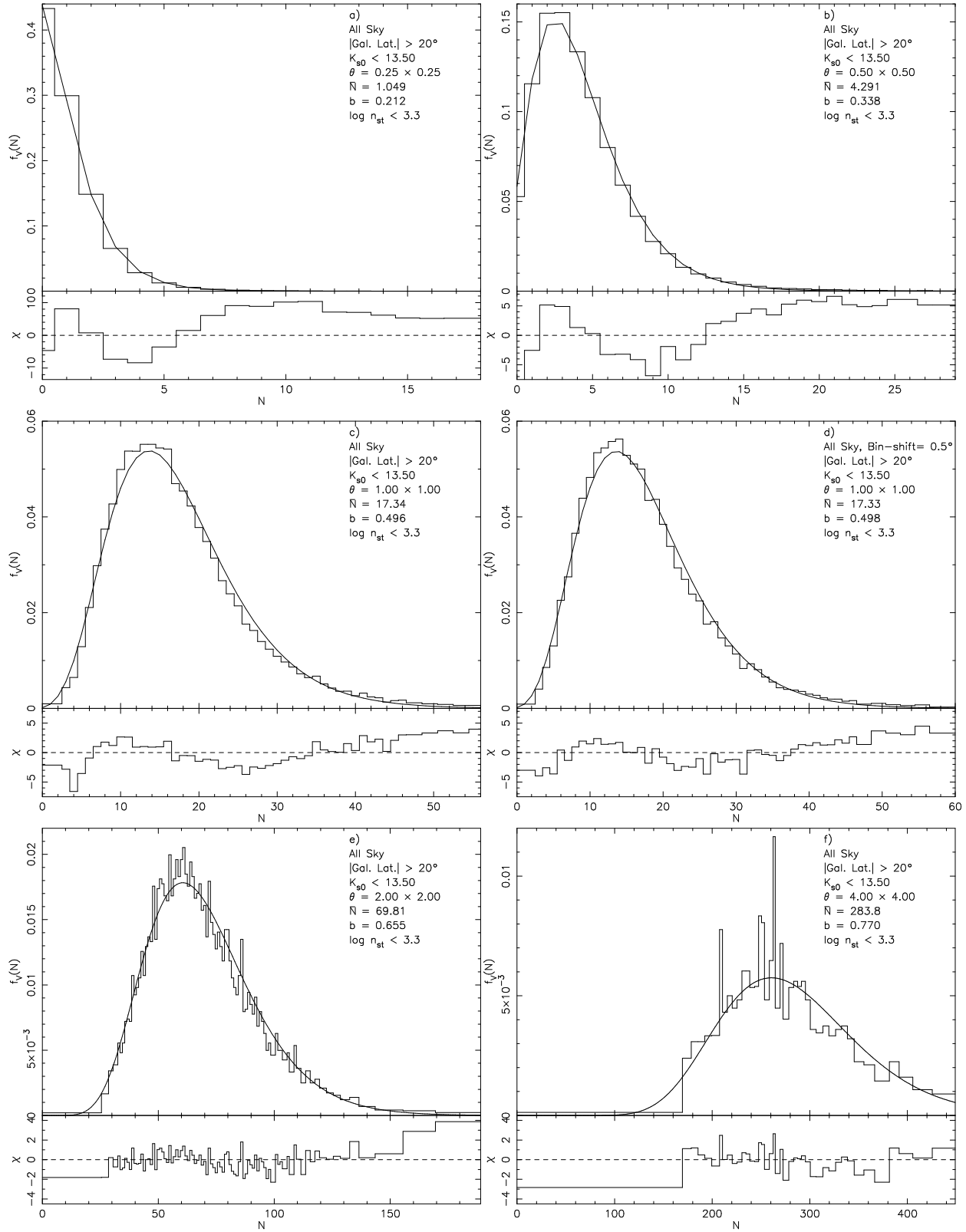


FIG. 2.— Least-squares fits (continuous lines) of $f_V(N)$ to the observed histograms for square cells of six different size cells on the sky. The area under the histograms in the bottom panel of each figure displays the values of χ for the fit. The plots exclude the final (high N 's) bin. In (d), the histogram was measured after shifting the bins by 0.5° in longitude.

culiarity of the unique configuration of large clusters in the Universe, our emphasis on fitting the overall distribution rather than giving greater weight to either the peak or tail, very small systematic effects in the 2MASS catalog and its analysis, or a real physical effect. If the last possibility is true, it might be caused by several effects including environmental interactions which tend to enhance the luminosities of very overdense regions, mergers in relatively overdense regions which enhance the number of cells around the peak of the distribution, a remnant of initial conditions when galaxies started clustering, or segregation of more massive galaxies into smaller volumes. Since the overall differences are so small, it will be a considerable challenge to determine their causes.

Figures 3a-d show variations of these counts in cells. The upper two comparisons are for $1^\circ \times 1^\circ$ cells (which we will now use for succeeding representative illustrations) over the entire sky, as before, but with magnitude cutoffs of $K_{s,0} < 12.5$ and $K_{s,0} < 13.0$. Examining the values of b for different magnitude cutoffs can describe whether magnitudes are partially correlated with position, as discussed in Section 4. Comparison with Figure 2 shows that the excellence of the fit is not much affected by the magnitude cutoff, as we would expect for a statistically complete sample. Figures 3c and 3d show samples with the standard magnitude cutoffs but confined to Galactic latitudes more than 45° and 70° from the Galactic plane. Comparison with the $1^\circ \times 1^\circ$ cells of Figures 2c and 2d, shows that the fits are as good and the values of b are the same within 2% for the 45° Galactic latitude cutoff and within 4% for the 70° cutoff. The 70° cutoff has larger fluctuations because it has only 20% of the number of cells as the 45° cutoff and less than 10% of the cells in the 20° cutoff. Evidently galactic obscuration is not a significant problem above $\pm 20^\circ$ latitude for these distribution functions.

The 2MASS sample is the first that is large enough for a precise determination of variations among different parts of the sky. Figures 4a - d give our results for dividing the sky into four independent quadrants. Each quadrant contains between about 5,500 and 6,200 usable cells. Fluctuations around equation (1) are very small, though naturally they differ in detail. Among these quadrants the variance of \bar{N} is 1.2% and of b is just 1.9%. For these quadrants divided into $4^\circ \times 4^\circ$ cells, for which each quadrant has between about 250 and 330 cells, the variance of \bar{N} is 1.5% and of b is 2.6%. The smaller fluctuations among the larger cells, which are more representative of the total galaxy distribution, partly compensate for the smaller total number of such cells. This suggests that a very conservative estimate of the uncertainty in b is 3%. By averaging the two quadrants with the lowest values of b to give 0.485 and comparing with the averages of the two quadrants giving the largest value of $b = 0.494$, we would obtain an estimate of 2% for the uncertainty of b in cells of one square degree. For comparison, earlier estimates of b from the catalogs mentioned in Section 1 gave uncertainties of 5-10% for b .

It is interesting to see the effects of a large cluster, in particular the Shapley Supercluster, on these statistics. On small scales it is obviously noticeable, as pointed out in the northwest quadrant of Figure 1. If it were important when averaged over the whole sky, or even over a

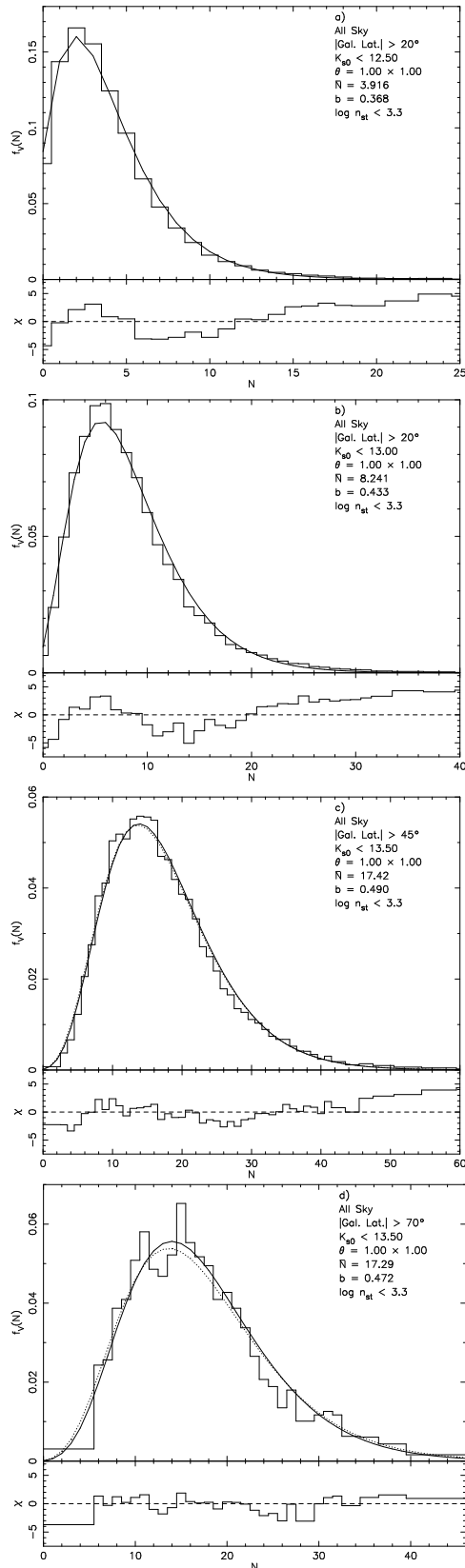


FIG. 3.— As Figure 2, except (a) and (b) indicate different magnitude cuts while (c) and (d) indicate different Galactic latitude cuts, all with 1° cells on the sky. The dotted lines in (c) and (d) indicate the best-fit model from the full sample with values of b and \bar{N} given in Table 1.

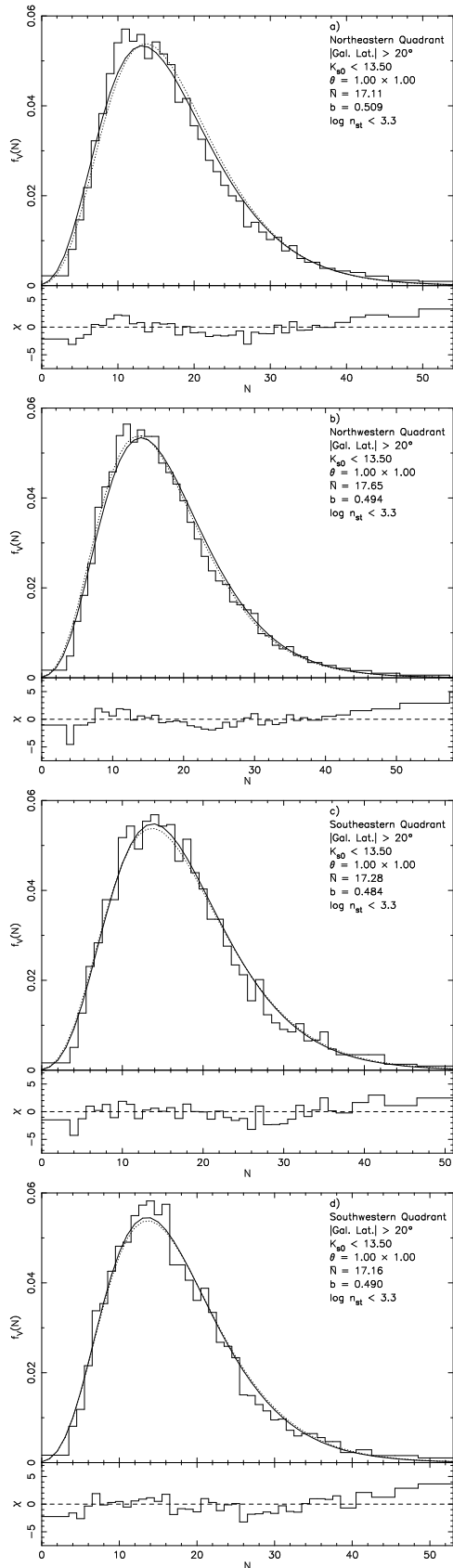


FIG. 4.— As Figure 2, except the figures indicate different quadrants all with 1° cells on the sky. The dotted lines indicate the best-fit model from the full sample with values of b and \bar{N} given in Table 1.

quadrant, we would consider it a sufficient anomaly to question whether it could have formed by gravitational many-body clustering alone, or whether it needed to arise from large perturbations in the early universe.

Figures 5a, b show the effects of removing the Shapley Supercluster from the all sky sample and from the northwest quadrant. This is effected by removing all cells within 10 degrees of $(\alpha_{gal}, \delta_{gal}) = (312.457^\circ, 30.754^\circ)$. Comparison with the same all sky samples in Figures 2c, d shows that removing the SSC reduces \bar{N} slightly, as expected, but reduces the value of b by less than 1%, and changes the histograms by less than the effects of the bin shift. On the smaller scale of a quadrant, however, there is less dilution and the effects of the SSC are more noticeable. The value of b is now reduced by 3%, compared with Figure 4b, although the histograms remain very similar.

A small fraction of anomalies in the 2MASS Galaxy (extended source) Catalog may be produced by contamination from point sources so close to each other that they masquerade as an extended source. For this to happen, their colors and magnitudes would also have to coincide with our criteria described in Section 2 for a galaxy. Figures 2c and 5c, d illustrate this effect. In Figure 5c we employ the less stringent criterion that all cells contain less than $10^{3.6}$ point sources, compared to limits of $10^{3.3}$ and $10^{3.0}$ in Figures 2c and 5d. This less stringent criterion induces slight fluctuations in the histograms but does not change the values of \bar{N} or b to three significant figures. The more stringent criterion of Figure 5d reduces both the number of cells and galaxies considerably (see Table 1 below) and has a 3% smaller value of b . This, and examination of Table 1, suggest that the limit of $10^{3.3}$ is a reasonable compromise.

In Figure 6, we directly compare a sample from the 2MASS Point Source Catalog (PSC, mainly stars) to a sample from the 2MASS XSC (mainly galaxies). To mitigate the effects of the Galactic disc, the comparison uses a Galactic latitude cutoff of 70° . In the PSC, we first selected objects with valid photometry in all three bands, where $K_{s,0} < 13.5$. Since there are many more objects in the PSC, we then randomly selected objects with a probability that would give approximately the same \bar{N} as seen in the same area as the XSC. We also used the same stellar density requirements. The two distributions (XSC - solid line, PSC - dotted line) are clearly different with the PSC showing much less clustering (lower b). We also found that reducing the \bar{N} for the PSC by magnitude selection produced a similar value of $b \approx 0.05$.

The dependence of b on the scale and shape of the cells incorporates important information about the two-galaxy correlation function, as indicated by equation (3). Through the form of equation (1), this dependence of b also incorporates much information about higher order correlations. This scale dependence can be used to test the applicability of computer simulations. Indeed a wide range of cold dark matter models do not agree with the scale dependence of b in the IRAS Catalog (Sheth et al. 1994). The increased precision of the 2MASS Catalog now makes $b(\theta)$ an even more stringent test of computer simulations. The $b(\theta)$ dependence is shown in Figure 7, where we have indicated conservative uncertainties of $\pm 3\%$ for each value of b . Typical CDM

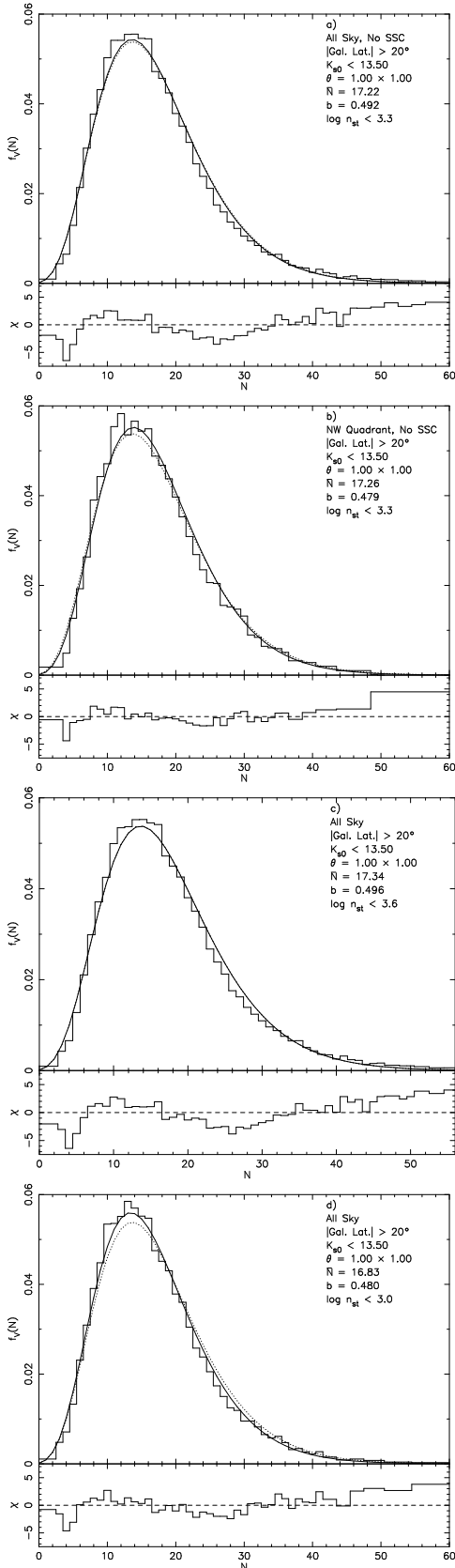


FIG. 5.— As Figure 2, except (a) and (b) indicate removing the Shapley Supercluster from the entire sky and the northwestern quadrant, while (c) and (d) indicate changing the stellar density at which cells are excluded, all with 1° size cells on the sky. The dotted lines indicate the best-fit model from the full sample with values of b and \bar{N} given in Table 1.

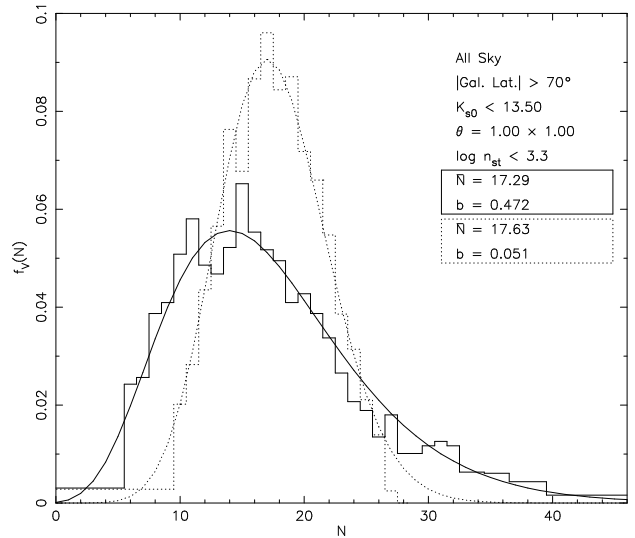


FIG. 6.— Least-squares fits (continuous lines) of $f_V(N)$ to the observed histograms for likely galaxies (2MASS XSC, solid lines) and likely stars (2MASS PSC, dotted lines).

models, especially those whose initial perturbation spectra produce large dark matter haloes that contain many galaxies, have too many voids and too many filaments at the present time (Baertschiger & Sylos-Labini 2004, private communication). Even if they agree approximately with the functional form of equation (1), their excessive voids and filamentary structures would give significantly greater values of b on small or large scales than the observations in Figure 7 show. In Figure 7, we also compare $b(\theta)$ with values based on the two-galaxy angular correlation function, $W(s)$. Lahav & Saslaw (1992) derived $b(\theta)$ for square cells of size $\omega = \theta \times \theta$ square degrees

$$b(\theta) = 1 - (1 + \bar{N} s_0^{\gamma-1} C_\gamma \theta^{5-\gamma})^{-0.5}, \quad (6)$$

where $W(s) = (s/s_0)^{1-\gamma}$, \bar{N} is the expected number of galaxies projected into a cell, and C_γ is a coefficient evaluated numerically from $J \equiv \iint_{\omega} \theta^{1-\gamma} d\omega_1 d\omega_2 = C_\gamma \theta^{5-\gamma}$ as in Totsuji & Kihara (1969) giving $C_\gamma = 2.25$ for $\gamma = 1.8$. Maller et al. (2005) find $\gamma = 1.79 \pm 0.02$ and $s_0 = 0.054 \pm 0.008$ for the 2MASS catalog at $K_{s,0} < 13.5$, from which we derive the dotted line in Figure 7. This fit is less good at smaller θ and has a $\chi^2 = 33.6$ for 5 degrees of freedom. Fitting γ and s_0 from $b(\theta)$, we find $\gamma = 1.81 \pm 0.04$ and $s_0 = 0.045 \pm 0.003$ (solid line in Figure 7), with a $\chi^2 = 3.0$, overlapping with the values from Maller et al. (2005). The distribution function, equation (1), therefore provides a good method for measuring the angular correlation function.

Table 1 below gives a more detailed summary of results for a wider range of analyses than Figures 2–7. The first section of Table 1 examines samples with different stellar density limits in $1 \times 1^\circ$ cells over all the unobscured sky above $\pm 20^\circ$ Galactic latitude but with different magnitude cutoffs. Values of \bar{N} and b are determined in three different ways. In the first column of values, \bar{N} is found exactly by averaging its value over all cells of each sample, and b is found from the variance of counts in these cells using equation (4). In the second column, \bar{N} is found as before but b is found using a least-squares fit

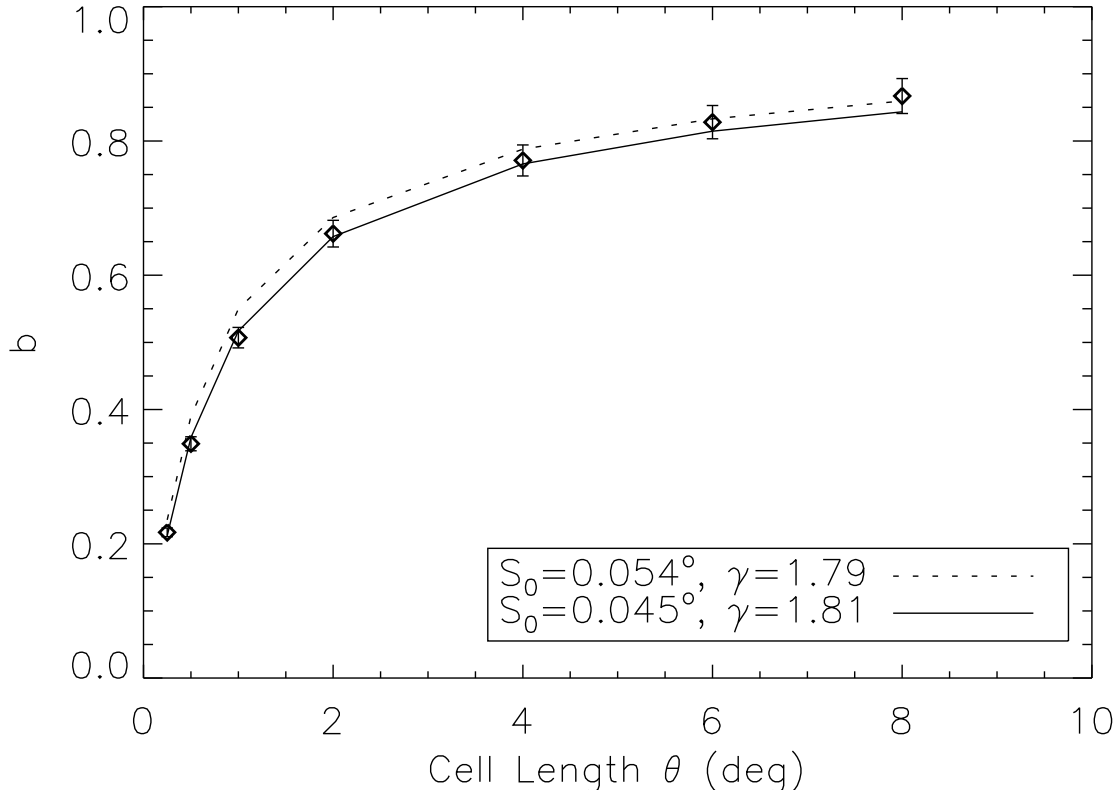


FIG. 7.— Plot of $b(\theta)$. The error bars represent conservative uncertainties of $\pm 3\%$ for each value of b . The predicted $b(\theta)$ (equation 6) for the two-galaxy angular correlation function as measured for 2MASS in Maller et al. (2005) (dotted-line) and in this paper (solid-line).

to equation (1). In the third column, \bar{N} and b are both obtained from a two-parameter least-squares fit to equation (1). In all cases, the fits are visually as good as those illustrated in Figures 2–5. We have also given values of χ^2 per degree of freedom, although as mentioned in Section 2 these values cannot be used to calculate absolute or relative probabilities for comparisons among themselves or with other distributions. Moreover, these χ^2 values tend to be dominated by the large N tail of the distributions. The values of b do not depend significantly on whether or not \bar{N} is a fitting parameter or is directly determined from the counts in cells. The values of b determined from the variance using equation (4) tend to be high for small scales but agree well with the values from the fits for larger cells which are more representative (even though there are fewer of them). The remaining sections of Table 1 examine the effects of varying Galactic latitude cutoffs, varying the size of the cell, and varying the regions of the sky to which the GQED is fit.

In Table 2, we compare the effects of sampling the galaxy catalog by magnitude cuts with sampling by a random selection that yields approximately the same number of galaxies at each magnitude cut. For these comparisons, we have used the usual stellar density cutoff ($n_{st} < 10^{3.3}$), All-sky region, and Galactic latitude cutoff (above $\pm 20^\circ$). The value of b in a subsample selected randomly with a probability p is related to the value of the parent sample by (e.g., Saslaw 2000)

$$(1 - b_{\text{subsample}})^2 = \frac{(1 - b_{\text{parent}})^2}{1 - (1 - p)(2 - b_{\text{parent}})b_{\text{parent}}}. \quad (7)$$

The values of b in Table 2 for the random sampling of the 13.5 magnitude limited galaxy catalog compared with the values of b in Table 1 confirm equation (7). The pairs of rows in Table 2 give observed parameters for a magnitude cut and for a corresponding Poisson selected subsample. This analysis is for cells of $1 \times 1^\circ$, $2 \times 2^\circ$, and $4 \times 4^\circ$. Figure 8 shows the differences between b measured for the magnitude cut and b for an equivalent randomly selected subsample.

The magnitude selected subsample always has a higher observed value of b than the corresponding randomly selected subsample. This effect appears to be mainly geometric. As one goes to brighter subsamples, their average volume decreases provided the distribution is statistically homogeneous. This affects $W(s)$ by increasing s_0 . Assuming the average radial distance sampled follows $D(m) \propto 10^{m/5}$, and with the usual scaling argument, $W(s) \propto W(s D(m))/D(m)$ (Peebles 1993),

$$s_{0,m_2} = s_{0,m_1} 10^{[(m_1 - m_2)/5][\gamma/(\gamma - 1)]}. \quad (8)$$

Combining equations 6 and 8, we can predict $b(\theta, m)$ based on $W(s)$ at $K_{s,0} = 13.5$. In Figure 9, we show the measured b minus this predicted b . Using the angular correlation, $W(s, 13.5)$, from Maller et al. (2005), there are some small discrepancies for small θ . With our best-fit $W(s, 13.5)$, there are no discrepancies.

4. SUMMARY AND DISCUSSION

Our main result is that at a level of precision 2-3 times better than possible with previous catalogs, the detailed

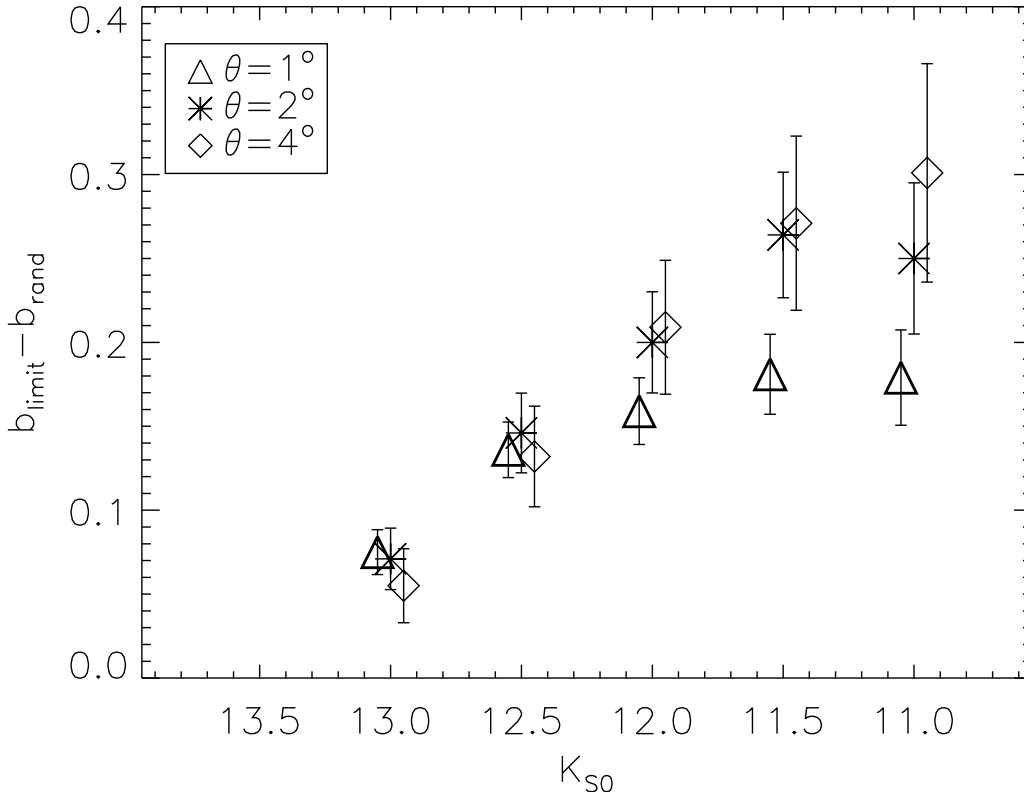


FIG. 8.— Plot of the differences between values of b measured from magnitude limited subsamples and from randomly selected subsamples of equal size as a function of magnitude for three cell sizes. Small shifts in plotted magnitude are made so that individual data-points and error bars can be distinguished. The error bars represent conservative uncertainties scaled by \bar{N} to $\pm 3\%$ of b for $K_{s,0} = 13.5$.

form of the galaxy distribution in the 2MASS Catalog agrees with its prediction from gravitational cosmological many-body theory. The value of the clustering parameter b in equation (3) appears to be $b = 0.867 \pm 0.026$ on large scales in the present universe with $z \lesssim 0.1$. This is in accordance with the value of 0.83 ± 0.05 for the much smaller but also highly complete three-dimensional Pisces-Perseus sample (Saslaw & Haque-Copilah 1998). Table 1 shows that as the cell size increases the values of b deduced from equation (4) agree better with the values in the χ^2 fits. This is essentially because larger cells are more representative of the global clustering, and their variance is more accurately determined. These values of b also agree with N-body simulations at the present time in $\Omega_0 = 1$ models (summarized in Saslaw 2000). Agreement with gravitational many-body theory need not have occurred at this level, especially since there are at least four major processes that could have destroyed it. The reasons that the agreement survives may be quite instructive.

First, a non-uniform distribution of dark gravitating matter that differs from the luminous galaxy distribution could significantly modify the observed galaxy distribution, in disagreement with the form of equation (1). If dark haloes contain many galaxies, the resulting voids and filaments could exceed those observed. The value of b in such models would be too high. Moreover models with overlapping individual dark matter haloes would soften the gravitational potential significantly and their result-

ing peculiar velocity distribution function would also disagree with observations (Leong & Saslaw 2004). All this indicates that when galaxies cluster most of the dark matter is located in the haloes of individual galaxies.

Second, if the initial perturbations that stimulated galaxy clustering have survived into the present non-linear regime, they could produce departures from the form of equation (1). This would be especially true if the initial conditions were strongly correlated or anti-correlated over large scales and have not had time to relax through a sequence of quasi-equilibrium states (Saslaw 2000). For example, an initial power law perturbation spectrum would have to have an exponent between $-1 \lesssim n \lesssim 1$ for such relaxation (Itoh 1990). Of course the initial power spectrum may not have been a simple power law; then this question becomes much more complicated and has not yet been systematically explored.

Third, there is considerable evidence, especially from the Hubble Deep Fields, that merging has played a significant role in galaxy formation which extends into the present. Merging tends to modify the form of $f_V(N)$ slightly and decrease the value of b (Fang & Saslaw 1997). The effects of merger induced starbursts modify the luminosity function, and complicate the selection of galaxies in the distribution function, probably depending on the local environment.

Evidently mergers do not destroy the distribution functions in Section 3. There may be several reasons for this.

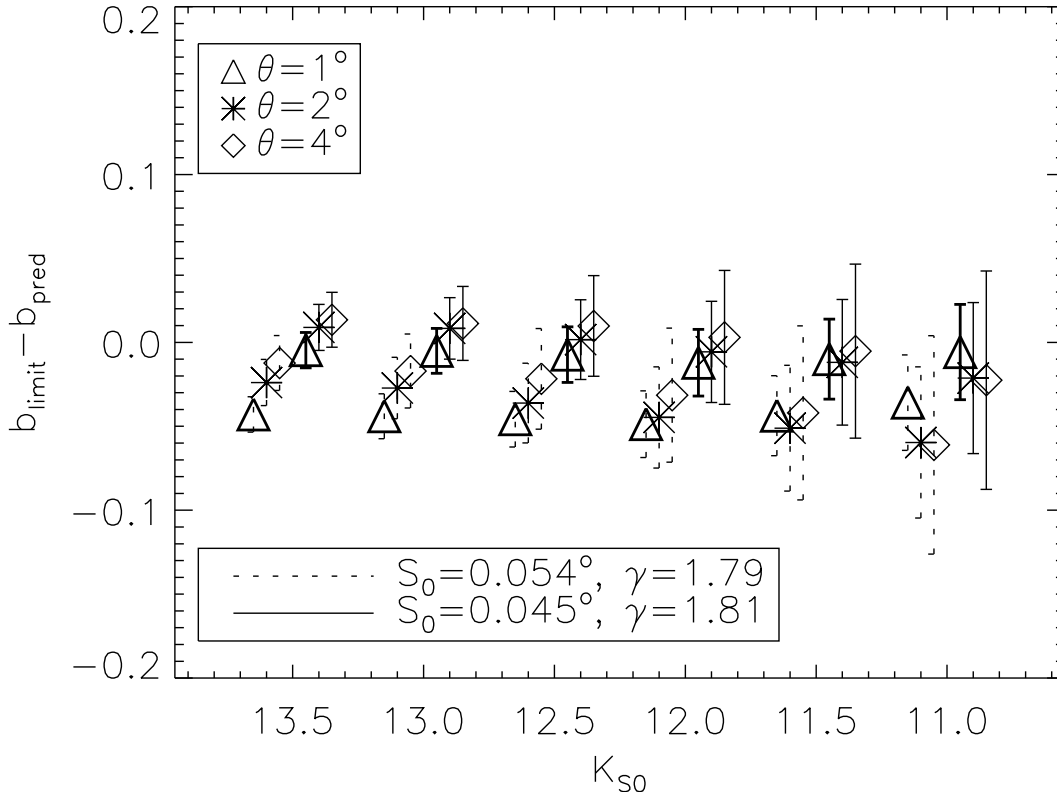


FIG. 9.— Plot of the differences between values of b measured from magnitude limited subsamples and predictions for b from equations 6 and 8 as a function of magnitude for three cell sizes. We use the two-galaxy angular correlation function as measured for 2MASS in Maller et al. (2005) (dotted error-bars) and in this paper (solid error-bars). Small shifts in plotted magnitude are made so that individual data-points and error bars can be distinguished. The error bars represent conservative uncertainties scaled by \bar{N} to $\pm 3\%$ of b for $K_{s,0} = 13.5$.

Although individual mergers may be dramatic, only a small percentage of galaxies merge at any given time so they do not have much effect on the overall statistics. When galaxies merge, they generally do so near the center of mass with their nearest neighbor. These centers of mass may have a distribution which approximately follows that of the galaxies themselves. Moreover intervals between mergers are often long compared with the local orbital relaxation time, so the merged galaxy has time to acquire the quasi-equilibrium distribution of equation (1).

Fourth, although the distribution of equation (1) is for systems in which all galaxies have the same mass, N-body simulations (e.g., Itoh et al. 1993) show that a range of masses generally enhances clustering and increases the value of b compared with single mass cases. The effect is relatively small, typically $\sim 10\%$, because much of the later clustering involves the collective interaction of individual galaxies with groups of galaxies, or of groups with other groups, for which the masses of individual galaxies are less relevant. For a wide range of masses, there is a tendency for massive galaxies to acquire less massive galaxies as satellites. How much this affects the distribution function depends on the relative total numbers of low and high mass galaxies and, for the observations, on detailed models of mass-luminosity galaxy selection.

While it is conceivable that these four, and perhaps other, effects might conspire to leave the distribution

function of equation (1) invariant, it seems more likely to us that each effect is individually small. Nonetheless they may be present to some degree since the fits to equation (1) are not perfect. In particular, there seem to be slight systematic tendencies for the observed peaks to exceed the theoretical peaks, for a small observed excess in the large N tail, and for a mild observed deficit between the peak and this tail. This holds for many samples, but not all. It seems somewhat more prominent in samples with greater stellar contamination, but might also be produced by some of the effects mentioned previously. At present, it seems that tracking down these small discrepancies will require a combination of even more extensive observations and more detailed models.

We have also found (Table 2) that values of b for subsamples limited by brighter apparent magnitude cutoffs are higher than b would be for a subsample selected randomly with the same probability. This was not evident in an earlier analysis (Saslaw & Crane 1991) of the Zwicky catalog, probably because this earlier catalog contains only about 7% as many galaxies as 2MASS and differences of ≤ 1 mag were explored. This effect can be explained almost entirely by the smaller volume of subsamples with brighter magnitude cutoffs, as Figure 9 shows. From equation (3), the spatially integrated effect of luminosity clustering as observed in the luminosity dependence of the two-point correlation function (e.g., Benoist et al. 1996; Mo et al. 1994; Norberg et al. 2001)

is therefore small. Similarly, the good fits of our magnitude limited subsamples to equation (1), which includes all the higher order correlation functions and moments of the distribution, show that luminosity clustering is small when averaged over large statistically homogeneous volumes containing many clusters. Physically, this would be expected if most of the clustering were produced by collective gravitational interactions (e.g., Saslaw 2000).

With further information about other properties of the 2MASS galaxies, distribution functions will make possible new insights into relative clusterings based on morphological types, colors, presence of satellite and tidally interacting galaxies, etc. This will contribute to a wealth of constraints on galaxy formation and evolution in more detailed models.

This publication makes use of data products from the Two Micron All Sky Survey, which is a joint project of the University of Massachusetts and the Infrared Processing and Analysis Center/California Institute of Technology, funded by the National Aeronautics and Space Administration and the National Science Foundation. We are especially grateful to Mike Skrutskie for helpful advice about the 2MASS survey and to the anonymous referee for especially helpful comments. GRS acknowledges the receipt of an Achievement Reward for College Scientists fellowship. Partial support was also provided by the F.H. Levinson Fund of the Peninsula Community Foundation.

REFERENCES

- Ahmad, F., Saslaw, W. C. and Bhat, N. I. 2002, *ApJ*, 571, 576
 Barkhouse, W. A. and Hall, P. B. 2001, *AJ*, 121, 2848
 Benoist, C., Maurogordato, S., da Costa, L. N., Cappi, A. and Schaeffer, R., 1996, *ApJ*, 472, 452
 Calabretta, M. R. and Greisen, E. W. 2002, *A&A*, 395, 1077
 Fang, F. and Saslaw, W. C., 1997, *ApJ*, 476, 534
 Fang, F. and Zou, Z., 1994, *ApJ*, 421, 9
 Fukushige, T. and Makino, J. 2003, *ApJ*, 588, 674
 Itoh, M., 1990, *PASJ*, 42, 481
 Itoh, M., Inagaki, S. and Saslaw, W. C., 1990, *ApJ*, 331, 45
 Itoh, M., Inagaki, S. and Saslaw, W. C., 1990, *ApJ*, 356, 315
 Itoh, M., Inagaki, S. and Saslaw, W. C., 1993, *ApJ*, 403, 476
 Kendall, M. and Stuart, A., 1979, *The Advanced Theory of Statistics*, 4th. ed. Chapter 30
 Lahav, O. and Saslaw, W. C., 1992, *ApJ*, 396, 430
 Leong, B. and Saslaw, W. C., 2004, *ApJ*, 608, 636
 Majewski, S. R., Skrutskie, M. F., Weinberg, M. D. and Ostheimer, J. C., 2003, *ApJ*, 599, 1082
 Maller, A. H., McIntosh, D. H., Katz, N. and Weinberg, M. D., 2004, *ApJ*, 619, 147
 Mo, H. J., McGaugh, S. S. and Bothun, G. D., */mnras*, 267, 129
 Norberg, P. et al., 2001, *MNRAS*, 328, 64
 Peebles, P. J. E., 1993, *Principles of Physical Cosmology* (Princeton Univ. Press)
 Saslaw, W. C., 2000, *The Distribution of the Galaxies: Gravitational Clustering in Cosmology*, (New York: Cambridge University Press)
 Saslaw, W. C. and Crane, P., 1991, *ApJ*, 380, 315
 Saslaw, W. C. and Edgar, J. H., 2000, *ApJ*, 534, 1
 Saslaw, W. C. and Fang, F., 1996, *ApJ*, 460, 16
 Saslaw, W. C. and Hamilton, A. J. S., 1984, *ApJ*, 276, 13
 Saslaw, W. C. and Haque-Copilah, S., 1998, *ApJ*, 509, 595
 Schlegel, D., Finkbeiner, D., and Davis, M. 1998, *ApJ*, 500, 525
 Sheth, R. K., Mo, H. J. and Saslaw, W. C., 1994, *ApJ*, 427, 562
 Totsuji, H. and Kihara, T., 1969, *PASJ*, 21, 221

TABLE 1. GQED FITS TO 2MASS DATA

Max K_{s0}	Max $\log(n_{st})$	Region	Min $ \delta_{Gal} $	θ	Total Galaxies	Total Cells	From Variance			Fitting b			Fitting \bar{N} & b		
							\bar{N}	b	χ^2/Dof	\bar{N}	b	χ^2/Dof	\bar{N}	b	χ^2/Dof
For Varying n_{st} , K_{s0} Cutoffs															
11.00	3.0	All	20	1.00	6717	15199	0.44	0.228	26.4/ 7	0.44	0.203	14.9/ 6	0.44	0.200	14.2/ 5
11.00	3.3	All	20	1.00	10940	23348	0.47	0.264	84.5/ 8	0.47	0.223	37.6/ 7	0.46	0.218	34.8/ 6
11.00	3.6	All	20	1.00	11421	24171	0.47	0.274	116.0/ 8	0.47	0.223	42.8/ 7	0.46	0.217	39.0/ 6
11.50	3.0	All	20	1.00	13655	15199	0.90	0.283	55.9/ 9	0.90	0.248	23.9/ 8	0.89	0.245	22.3/ 7
11.50	3.3	All	20	1.00	22252	23348	0.95	0.329	250.8/12	0.95	0.266	87.3/11	0.92	0.257	76.7/10
11.50	3.6	All	20	1.00	23131	24171	0.96	0.333	288.8/12	0.96	0.265	91.7/11	0.93	0.256	79.3/10
12.00	3.0	All	20	1.00	27872	15199	1.83	0.340	158.5/13	1.83	0.291	72.9/12	1.79	0.284	66.6/11
12.00	3.3	All	20	1.00	45385	23348	1.94	0.388	479.2/17	1.94	0.317	166.8/16	1.88	0.305	144.5/15
12.00	3.6	All	20	1.00	47145	24171	1.95	0.389	505.4/17	1.95	0.317	169.6/16	1.88	0.305	145.6/15
12.50	3.0	All	20	1.00	58035	15199	3.82	0.398	193.0/20	3.82	0.355	94.8/19	3.75	0.349	88.0/18
12.50	3.3	All	20	1.00	94467	23348	4.05	0.453	731.8/24	4.05	0.382	243.3/23	3.92	0.368	209.6/22
12.50	3.6	All	20	1.00	97926	24171	4.05	0.453	751.8/24	4.05	0.382	247.3/23	3.92	0.369	212.5/22
12.75	3.0	All	20	1.00	84186	15199	5.54	0.432	204.7/25	5.54	0.392	98.8/24	5.46	0.386	92.7/23
12.75	3.3	All	20	1.00	136610	23348	5.85	0.485	836.6/29	5.85	0.417	264.1/28	5.69	0.405	232.3/27
12.75	3.6	All	20	1.00	141599	24171	5.86	0.485	851.7/29	5.86	0.417	268.0/28	5.70	0.406	235.6/27
13.00	3.0	All	20	1.00	122608	15199	8.07	0.461	271.4/31	8.07	0.422	143.9/30	7.95	0.416	136.1/29
13.00	3.3	All	20	1.00	197738	23348	8.47	0.514	1108.0/37	8.47	0.446	364.2/36	8.24	0.433	326.3/35
13.00	3.6	All	20	1.00	204826	24171	8.47	0.514	1111.1/37	8.47	0.447	366.9/36	8.25	0.434	328.1/35
13.25	3.0	All	20	1.00	178009	15199	11.71	0.492	264.8/38	11.71	0.456	138.3/37	11.55	0.450	129.6/36
13.25	3.3	All	20	1.00	285786	23348	12.24	0.540	1073.2/45	12.24	0.479	359.9/44	11.94	0.467	320.5/43
13.25	3.6	All	20	1.00	296039	24171	12.25	0.540	1082.8/46	12.25	0.479	369.2/45	11.95	0.467	328.2/44
13.50	3.0	All	20	1.00	258815	15199	17.03	0.520	308.5/47	17.03	0.485	168.0/46	16.83	0.480	159.9/45
13.50	3.1	All	20	1.00	333937	19170	17.42	0.541	617.0/52	17.42	0.495	275.6/51	17.14	0.487	256.9/50
13.50	3.2	All	20	1.00	382096	21652	17.65	0.554	831.0/54	17.65	0.504	346.7/53	17.32	0.495	318.9/52
13.50 ^a	3.3	All	20	1.00	413339	23348	17.70	0.565	1126.1/54	17.70	0.507	397.7/53	17.34	0.496	359.9/52
13.50	3.4	All	20	1.00	422901	23894	17.70	0.564	1130.7/55	17.70	0.507	404.5/54	17.33	0.497	365.9/53
13.50	3.5	All	20	1.00	427446	24136	17.71	0.563	1142.7/56	17.71	0.507	408.4/55	17.34	0.496	369.0/54
13.50	3.6	All	20	1.00	428109	24171	17.71	0.563	1137.5/56	17.71	0.507	406.5/55	17.34	0.496	367.2/54
13.50	4.0	All	20	1.00	428578	24194	17.71	0.563	1142.0/56	17.71	0.507	408.1/55	17.34	0.497	368.5/54
For Varying Galactic Latitude Cutoffs															
13.50 ^a	3.3	All	20	1.00	413339	23348	17.70	0.565	1126.1/54	17.70	0.507	397.7/53	17.34	0.496	359.9/52
13.50	3.3	All	45	1.00	203044	11439	17.75	0.550	452.0/48	17.75	0.499	181.3/47	17.42	0.490	165.2/46
13.50	3.3	All	70	1.00	39548	2223	17.79	0.555	187.1/32	17.79	0.488	92.6/31	17.29	0.472	85.7/30
For Varying θ															
13.50	3.3	All	20	0.25	439754	412101	1.07	0.258	2266.4/19	1.07	0.217	975.6/18	1.05	0.212	897.9/17
13.50	3.3	All	20	0.50	430439	98048	4.39	0.406	2069.1/31	4.39	0.349	774.9/30	4.29	0.338	688.3/29
13.50 ^a	3.3	All	20	1.00	413339	23348	17.70	0.565	1126.1/54	17.70	0.507	397.7/53	17.34	0.496	359.9/52
13.50 ^a	3.3	All	20	2.00	384240	5409	71.04	0.697	272.8/93	71.04	0.662	138.0/92	69.81	0.655	126.1/91
13.50 ^a	3.3	All	20	4.00	330298	1159	284.99	0.793	91.7/43	284.99	0.771	61.7/42	283.80	0.770	61.4/41
13.50	3.3	All	20	6.00	280916	435	645.78	0.835	13.4/17	645.78	0.828	11.7/16	643.56	0.828	11.6/15
13.50	3.3	All	20	8.00	231854	201	1153.50	0.858	3.5/ 7	1153.50	0.867	2.6/ 6	1154.00	0.867	2.6/ 5
For Varying Regions of the Sky Using $\theta = 1^\circ$ Cells															
13.50 ^a	3.3	All	20	1.00	413339	23348	17.70	0.565	1126.1/54	17.70	0.507	397.7/53	17.34	0.496	359.9/52
13.50	3.3	All	20	1.00 ^b	413308	23365	17.69	0.562	995.5/55	17.69	0.508	352.6/54	17.33	0.498	314.7/53
13.50	3.3	All ^c	20	1.00	404863	23050	17.56	0.554	951.0/54	17.56	0.502	374.4/53	17.22	0.492	341.0/52
13.50	3.3	N	20	1.00	217041	12220	17.76	0.573	681.0/49	17.76	0.512	221.7/48	17.39	0.502	202.0/47
13.50	3.3	S	20	1.00	196298	11128	17.64	0.553	501.7/48	17.64	0.500	231.9/47	17.24	0.489	210.5/46
13.50	3.3	E	20	1.00	201571	11465	17.58	0.561	523.1/48	17.58	0.509	221.0/47	17.21	0.498	202.8/46
13.50	3.3	W	20	1.00	210012	11786	17.82	0.566	643.1/49	17.82	0.504	203.8/48	17.43	0.493	181.6/47
13.50	3.3	NW	20	1.00	111595	6219	17.97	0.562	327.6/42	17.97	0.501	103.4/41	17.65	0.494	97.1/40
13.50	3.3	NW ^c	20	1.00	103119	5921	17.42	0.520	327.6/39	17.42	0.483	76.6/38	17.26	0.479	47.7/37
13.50	3.3	NE	20	1.00	104720	5958	17.58	0.584	370.9/41	17.58	0.523	138.4/40	17.11	0.509	124.3/39

TABLE 1. GQED FITS TO 2MASS DATA— *Continued*

Max K_{s0}	Max $\log(n_{st})$	Region	Min $ \delta_{Gal} $	θ	Total Galaxies	Total Cells	From Variance			Fitting b			Fitting \bar{N} & b		
							\bar{N}	b	χ^2/Dof	\bar{N}	b	χ^2/Dof	\bar{N}	b	χ^2/Dof
13.50	3.3	SE	20	1.00	96851	5507	17.59	0.532	198.5/40	17.59	0.493	131.1/39	17.28	0.484	124.4/38
13.50	3.3	SW	20	1.00	98417	5567	17.68	0.570	362.7/42	17.68	0.505	142.0/41	17.16	0.490	124.0/40
For Varying Regions of the Sky Using $\theta = 4^\circ$ Cells															
13.50 ^a	3.3	All	20	4.00	330298	1159	284.99	0.793	91.7/43	284.99	0.771	61.7/42	283.81	0.770	61.4/41
13.50	3.3	NW	20	4.00	95024	328	289.71	0.797	16.2/12	289.71	0.776	11.3/11	286.57	0.773	10.8/10
13.50	3.3	NE	20	4.00	83880	294	285.31	0.817	8.1/11	285.31	0.802	5.4/10	282.30	0.799	5.0/ 9
13.50	3.3	SE	20	4.00	71567	253	282.87	0.756	2.7/ 9	282.87	0.747	2.4/ 8	279.20	0.742	1.7/ 7
13.50	3.3	SW	20	4.00	73875	264	279.83	0.783	14.8/10	279.83	0.771	13.7/ 9	275.24	0.765	12.7/ 8

NOTE. — The units of n_{st} are deg^{-2} . The units of δ_{Gal} and θ are deg.

^a This row is a parent sample for randomly selected subsamples in Table 2.

^b The Galactic longitude bins were shifted by 0.5° for this fit.

^c Cells containing galaxies within 10 degrees the Shapley Supercluster were excluded for this fit.

TABLE 2. COMPARISON OF MAGNITUDE SELECTED SUBSAMPLES WITH RANDOMLY SELECTED SUBSAMPLES

Max K_{s0}	Poisson Prob.	θ	Total Galaxies	Total Cells	From Variance			Fitting b			Fitting \bar{N} & b		
					\bar{N}	b	χ^2/Dof	\bar{N}	b	χ^2/Dof	\bar{N}	b	χ^2/Dof
For Varying K_{s0} Cutoffs Compared to Random Selection from $K_{s0} = 13.50$ Cutoff Using $\theta = 1^\circ$ Cells													
11.00	1.0000	1.00	10940	23348	0.47	0.264	84.5/ 8	0.47	0.223	37.6/ 7	0.46	0.218	34.8/ 6
13.50	0.0265	1.00	10917	23348	0.47	0.049	12.1/ 5	0.47	0.044	11.2/ 4	0.47	0.043	11.1/ 3
11.50	1.0000	1.00	22252	23348	0.95	0.329	250.8/12	0.95	0.266	87.3/11	0.92	0.257	76.7/10
13.50	0.0538	1.00	22343	23348	0.96	0.091	13.3/ 8	0.96	0.085	11.4/ 7	0.95	0.084	11.3/ 6
12.00	1.0000	1.00	45385	23348	1.94	0.388	479.2/17	1.94	0.317	166.8/16	1.88	0.305	144.5/15
13.50	0.1100	1.00	45530	23348	1.95	0.188	87.5/12	1.95	0.158	45.2/11	1.93	0.157	43.2/10
12.50	1.0000	1.00	94467	23348	4.05	0.453	731.8/24	4.05	0.382	243.3/23	3.92	0.368	209.6/22
13.50	0.2290	1.00	94631	23348	4.05	0.292	278.1/19	4.05	0.246	142.6/18	4.00	0.241	132.2/17
13.00	1.0000	1.00	197738	23348	8.47	0.514	1108.0/37	8.47	0.446	364.2/36	8.24	0.433	326.3/35
13.50	0.4780	1.00	197645	23348	8.47	0.425	604.3/33	8.47	0.371	262.7/32	8.31	0.362	239.9/31
For Varying K_{s0} Cutoffs Compared to Random Selection from $K_{s0} = 13.50$ Cutoff Using $\theta = 2^\circ$ Cells													
11.00	1.0000	2.00	10111	5409	1.87	0.390	49.3/12	1.87	0.352	29.6/11	1.82	0.344	27.3/10
13.50	0.0263	2.00	10279	5409	1.90	0.112	10.3/ 8	1.90	0.102	9.2/ 7	1.90	0.102	9.1/ 6
11.50	1.0000	2.00	20585	5409	3.81	0.465	85.9/18	3.81	0.418	38.2/17	3.71	0.409	34.5/16
13.50	0.0536	2.00	20859	5409	3.86	0.179	25.3/13	3.86	0.154	16.9/12	3.84	0.152	16.5/11
12.00	1.0000	2.00	42092	5409	7.78	0.537	205.3/27	7.78	0.481	95.8/26	7.53	0.467	85.7/25
13.50	0.1100	2.00	42268	5409	7.81	0.309	34.7/20	7.81	0.281	20.9/19	7.76	0.279	20.0/18
12.50	1.0000	2.00	87685	5409	16.21	0.603	297.3/41	16.21	0.547	127.1/40	15.69	0.532	111.0/39
13.50	0.2280	2.00	87784	5409	16.23	0.450	162.2/34	15.23	0.401	84.5/33	16.02	0.394	79.7/32
13.00	1.0000	2.00	183757	5409	33.97	0.656	342.5/61	33.97	0.610	164.9/60	33.15	0.599	150.2/59
13.50	0.4780	2.00	183759	5409	33.97	0.579	203.4/56	33.97	0.539	114.1/55	33.43	0.532	104.5/54
For Varying K_{s0} Cutoffs Compared to Random Selection from $K_{s0} = 13.50$ Cutoff Using $\theta = 4^\circ$ Cells													
11.00	1.0000	4.00	8509	1159	7.34	0.546	37.3/17	7.34	0.504	22.7/16	7.19	0.496	21.9/15
13.50	0.0258	4.00	8517	1159	7.35	0.217	12.4/14	7.35	0.203	11.8/13	7.32	0.202	11.7/12
11.50	1.0000	4.00	17430	1159	15.04	0.610	55.1/24	15.04	0.575	40.3/23	14.63	0.564	38.2/22
13.50	0.0528	4.00	17385	1159	15.00	0.325	23.2/20	15.00	0.304	21.2/19	14.93	0.301	21.0/18
12.00	1.0000	4.00	35665	1159	30.77	0.674	96.1/35	30.77	0.633	64.0/34	29.95	0.622	60.9/33
13.50	0.1080	4.00	35619	1159	30.73	0.449	53.2/29	30.73	0.424	49.1/28	30.47	0.420	48.3/27
12.50	1.0000	4.00	74812	1159	64.55	0.725	78.9/35	64.55	0.689	40.9/34	63.61	0.683	39.6/33
13.50	0.2260	4.00	74913	1159	64.64	0.591	57.8/33	64.64	0.557	41.7/32	64.45	0.555	41.6/31
13.00	1.0000	4.00	157519	1159	135.91	0.764	77.1/39	135.91	0.735	40.4/38	134.46	0.731	39.4/37
13.50	0.4770	4.00	157197	1159	135.63	0.708	66.5/39	135.63	0.680	43.8/38	134.58	0.677	42.9/37

NOTE. — All fits were to All-sky data where $n_{st} < 3.3 \text{ deg}^{-2}$ and $|\delta_{Gal}| > 20 \text{ deg}$. The units of θ are deg.